Journal of Structural Geology 42 (2012) 163–170

Contents lists available at SciVerse ScienceDirect

Journal of Structural Geology

journal homepage: www.elsevier.com/locate/jsg

Viscoelastic damage modeling of sinkhole formation

Eyal Shalev*, Vladimir Lyakhovsky

Geological Survey of Israel, 30 Malkhe Israel, Jerusalem 95501, Israel

ARTICLE INFO

Article history:
Received 6 February 2012
Received in revised form
3 May 2012
Accepted 17 May 2012
Available online 7 June 2012

Keywords:
Sinkholes
Damage
Viscoelasticity
Modeling

ABSTRACT

The sinkholes along the Dead Sea coast are observed in two main sedimentary environments: alluvial fan sinkholes, which usually form abruptly as deep (~20 m) and narrow (~3 m) sinkholes, and mud-flat sinkholes, which usually form as shallow (a few centimeters) and wide (>5 m) sinkholes and deepen later. The mechanical collapse of all sinkholes is triggered by cavities created by the dissolution of an underlying salt layer by relatively fresh groundwater. The processes attributed to the mechanical formation of the sinkholes are viscous flow and brittle fracture failure. We use a two-dimensional viscoelastic damage rheology numerical model to quantitatively explain the brittle and ductile aspects of collapsed sinkholes. Three cases of the rheology of the collapsed sediments are simulated, 1) damage controlled failure, 2) viscoelastic controlled failure, and 3) an intermediate damage-viscoelastic case. Results show that viscoelasticity cannot be the sole process acting on the deformed layer because all sinkholes are characterized by sharp boundaries. The damage accumulation progresses until arched cavities are created in the soil layer. Because of the geometric heterogeneity of the layer (represented by the heterogeneity of the mesh) smaller blocks continue to fall after the first breakup into the cavity, advancing the arched cavity upwards. This propagation finally stops when the cavity is shallow enough to hold the irregular arch. The combination of these two processes creates competition within the stress reduction mechanism that may lead to either magnified or reduced deformation. The deformation is magnified in high shear stress locations, where the dispersion of the viscous flow spreads damage failure, and it is reduced in low shear stress locations where viscous flow disperses shear stress before the onset of damage.

1. Introduction

Formation of sinkholes is a widely observed phenomenon, occurring in many parts of the world. The mechanism that is responsible for the appearance of sinkholes is the dissolution of soluble rocks and the creation of subsurface cavities that collapse when not sufficiently supported (Martinez et al., 1998; Gutierrez and Cooper, 2002; Waltham et al., 2005; Parise, 2008). Sinkholes began to appear along the Dead Sea coast in Israel and Jordan in the early 1980's (Fig. 1). Sinkhole development has significantly accelerated since 2000; from 70 sinkholes/year in 2000 to 400 sinkholes/year in 2009, resulting in more than 2500 sinkholes (Abelson et al., 2006). The sinkholes are not uniformly scattered along the Dead Sea shores, but rather occur as clusters. Presently, 40 sinkhole sites are known along a narrow coastal strip, ~60 km long and 20–1000 m wide, which stretches from the water line westward. The number of sinkholes at each site ranges from 1 to around 100.

This regional-scale collapse is attributed to the rapid decline of the Dead Sea level (~1 m/y) (Yechieli et al., 2006). The decline of the Dead Sea reflects human activities such as interception of freshwater supply from the Jordan River and the maintenance of large evaporation ponds by the Dead Sea mineral industries in Jordan and Israel. Because of the recession of the Dead Sea level, and the decline in the fresh/saline water interface along the shore, brines that previously occupied salt layers below this interface are now being flushed out by relatively fresh groundwater that dissolves the salt and creates voids. The collapse of these voids creates the sinkholes. Abelson et al. (2006) showed that the sinkholes appear along lineaments, and based on seismic reflection profiles and InSAR measurements they concluded that the sinkholes track young fault systems. The faults serve as conduits, channeling freshwater from the deeper aquifer to the shallower one, promoting the development of sinkholes. Shalev et al. (2006) numerically simulated the dissolution of the salt layer and the creation of cavities. They showed the growth of the cavities from the bottom of the salt layer to the top and suggested that shortly after the cavities reach the top of the salt layer it collapses and creates sinkholes.

The sinkholes are observed in two main sedimentary environments along the western coast of the Dead Sea, which are mud-flats and alluvial fans. The alluvial fans are made of coarse gravel

* Corresponding author. Tel.: +972 2 5314 230.
E-mail address: eyal@gsi.gov.il (E. Shalev).

0191-8141/$ – see front matter © 2012 Elsevier Ltd. All rights reserved.
http://dx.doi.org/10.1016/j.jsg.2012.05.010

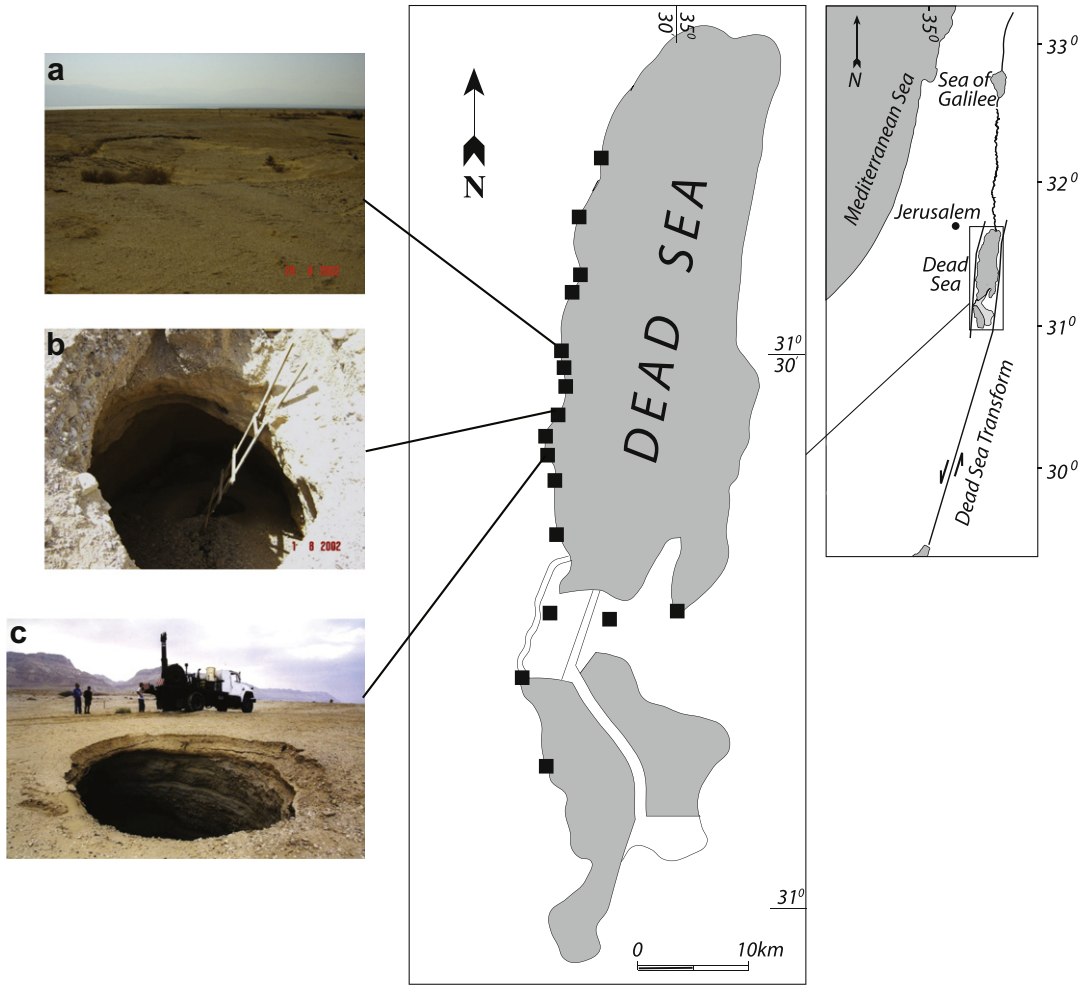

Fig. 1. Location map of the Dead Sea and sinkhole sites. Three types of sinkholes are shown: a) sinkhole in the mud flats soon after its collapse, b) sinkhole in alluvial fan, c) sinkhole in a mixed gravel-mud lithology.

alternating with fine-grained sediments (silt and clay), whereas the mud flats are mainly fine-grained sediments. The collapse-sinkholes in the alluvial fans tend to form abruptly and create a deep structure, sometimes reaching a depth of ~20 m. In the wet mud-flats, the sinkholes may show some surface ductile sagging prior to their collapse, and therefore are classified as sagging-collapse sinkholes (Gutierrez et al., 2008). These sinkholes form shallow (few cm) and wide (tens of meters) structures that might grow slowly to depths of 10 m (Fig. 2). The growth of the sinkhole is attributed to more dissolution or removal of the cavity fill by groundwater transport. This process is slow and might continue for years with a rate of ~10 cm/month.

Although the stability of sinkholes has been studied before (Tharp, 1999; Augarde et al., 2003; Parise and Lollino, 2011; Baryakh and Fedoseev, 2011), the transient deformation that creates sinkholes has not yet been studied. In this paper we study the mechanical processes that control cavity collapse at the Dead Sea coast. We simulate the two end member formation types of sinkholes (mud-flats and alluvial fans) with visco-elastic and damage modeling, and we study the inter-play between these two processes.

2. Dead Sea basin: geological background

The Dead Sea is the lowest place on continental Earth, 425 m below mean sea level (bmsl) in 2012; the deepest point in the basin is ~720 m bmsl (maximum water depth of ~300 m). It is located within the Dead Sea basin with an overall length of ~150 km, width of 15–20 km, and subsidence of more than 10 km. The mechanism for the basin formation is still controversial and is attributed to either a "pull apart" (e.g., Garfunkel, 1997) or "drop down" (e.g., Ben-Avraham et al., 2010).

The western margin of the Dead Sea basin is governed by a bimodal distribution of fault strikes, which form an orthorhombic pattern of zigzagging rift walls (Sagy et al., 2003). The uplifted margins of the basin are built of Precambrian basement rocks overlain by Paleozoic to Cenozoic sedimentary rocks. During the Miocene and through to Holocene times, mostly lacustrine and terrestrial sediments have accumulated within the basin (Zak, 1967). The upper tens of meters along the Dead Sea shores consist of the late Pleistocene Lisan Formation (Begin et al., 1974; Sneh, 1979) and the Holocene Ze'elim Formation (Manspeizer, 1985; Yechieli et al., 1993), which are composed of alternating clastic material (clay, sand, and gravel) deposited in fan deltas, with intercalations of lacustrine sediments (clay, aragonite, gypsum, and halite). The relative abundance of fine-grained layers within both formations increases eastward. The width of the coastal plain varies from ~5 km at the Ze'elim fan to <1 km in the Enot Zuqim area. The sinkholes develop within the sediments of the Ze'elim Formation and are confined to a narrow strip that stretches up to several hundred meters away from the shoreline. The salt layer has

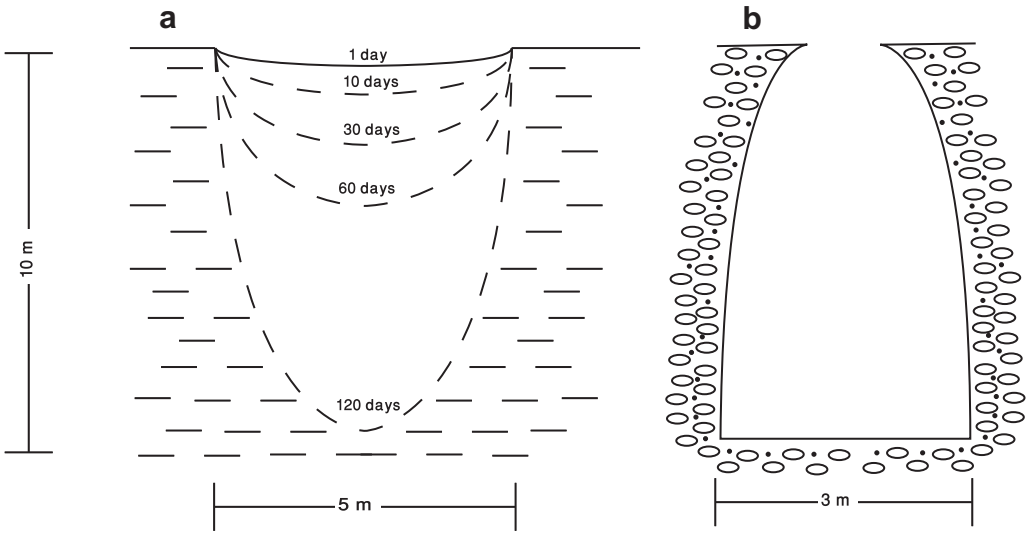

Fig. 2. a) Mud-flat sinkhole evolution. The sinkhole is formed with a relatively large radius (>5 m) and a small vertical displacement. With time the sinkholes deepens and may reach depths of 10 m b) Alluvial-fan sinkhole. The sinkhole is formed as a narrow deep sinkhole.

a thickness of ~20 m and the top of the salt layer is at depth of ~20 m below the surface. On top of the salt layer there is either a layer of mud in the mud flat areas, or gravel in the alluvial fans.

3. Formulation

We use a viscoelastic damage rheology model that quantitatively explains general aspects of brittle and ductile rock deformation. Maxwell's formulation describes the total strain tensor, ε_{ij}^{T}, as the sum of elastic-damage strain, ε_{ij}^{d}, and the viscous strain, ε_{ij}^{v}:

$$\varepsilon_{ij}^{T} = \varepsilon_{ij}^{d} + \varepsilon_{ij}^{v} \tag{1}$$

The viscous strain is governed by the exponential relation between the shear stress and the strain rate (Mitchell and Soga, 2005):

$$\dot{\varepsilon}_{ij}^{v} = \tau_{ij} A \exp\left(B\tau\right) \tag{2}$$

where τ_{ij} is the deviator stress, $\tau = \sqrt{(\tau_{ij}\tau_{ij})/2}$, the parameters A and B are empirical constants. Mitchell and Soga (2005) showed that for soils, B is about 10^{-5} Pa^{-1}, and A depends on the elapsed time of creep. We extrapolated the data given in Mitchell and Soga (2005) for an elapsed time of <1000 min to the elapsed time of the sinkhole formation process (10–100 days) to give values of $A = 10^{-12}$–10^{-16} (Pa s)$^{-1}$ where $A = 10^{-12}$ (Pa s)$^{-1}$ represents the viscous controlled process and $A = 10^{-16}$ (Pa s)$^{-1}$ represents the elastic-damage controlled process. The elapsed time of the sinkhole formation was measured in two independent observations: a) the time from the discovery of a cavity to its collapse was about three months, and b) the gradual subsidence of a collapse-sinkhole in the mud-flats after its initial collapse was ~10 cm/week.

The damage rheology model (Lyakhovsky et al., 2011) allows the calculation of the simultaneous evolution of damage, α, and its localization into narrow highly damaged zones (faults), seismic events, and associated deformation fields. It accounts for the evolution of the damage state variable α, as a function of the ongoing deformation, which control the effective elastic moduli and material degradation/healing. It also accounts for macroscopic brittle instability at a critical level of damage and related rapid conversion of elastic strain to permanent inelastic strain.

The nonlinear stress–strain relation for the elastic-damage term is (Hamiel et al., 2011):

$$\sigma_{ij} = \left(\lambda I_1 - \gamma\sqrt{I_2}\right)\delta_{ij} + \left(2\mu - \gamma\frac{I_1}{\sqrt{I_2}}\right)\varepsilon_{ij} \tag{3}$$

where $I_1 = \varepsilon_{kk}$ and $I_2 = \varepsilon_{ij}\varepsilon_{ij}$ are the first and second invariants of the elastic strain tensor ε_{ij}, λ and μ are the Lamé parameters of linear Hookean elasticity, and γ is a third modulus for a damaged solid. Below the onset of damage, $\gamma = 0$ and Eq. (3) reduces to the Hookean linear elastic formulation. With damage, the moduli λ, μ and γ are dependant on an evolving damage state variable $0 \le \alpha \le 1$. The transition from damage accumulation to healing is controlled by the value of the strain invariants ratio $\xi = I_1/\sqrt{I_2}$ which is connected to the internal friction angle of Byerlee's law (Byerlee, 1978). The value $\xi = \xi_0$ controls the transition from healing to damage accumulation. The rate of damage/healing accumulation is given by Lyakhovsky et al. (1997)):

$$\frac{d\alpha}{dt} = \begin{cases} C_d I_2(\xi - \xi_0) & \text{for} \quad \xi > \xi_0 \\ C_1 \exp\left(\dfrac{\alpha}{C_2}\right) I_2(\xi - \xi_0) & \text{for} \quad \xi < \xi_0 \end{cases}. \tag{4}$$

where the coefficient C_d gives the rate of positive damage evolution (material degradation) and is constrained by laboratory fracturing experiments (Lyakhovsky et al., 1997; Hamiel et al., 2004, 2009). The rate of damage recovery (material healing) is assumed to depend exponentially on α. This produces logarithmic healing with time in agreement with the behavior observed in laboratory experiments (e.g., Dieterich and Kilgore, 1996; Scholz, 2002; Johnson and Jia, 2005) with rocks and other materials. The evolving damage state variable α is calculated by the integration of $d\alpha/dt$ in time. We assume that the elastic moduli depend linearly on damage (Agnon and Lyakhovsky, 1995):

$$\begin{aligned} \lambda &= \text{const.} \\ \mu &= \mu_0 + \gamma_r \xi_0 \alpha \\ \gamma &= \gamma_r \alpha \end{aligned} \tag{5}$$

where μ_0 is the initial shear modulus and γ_r is constant.

Both the processes of viscous flow and damage accumulation may act separately to reduce shear stress. However, the two

processes are different in nature. The viscous flow reduces the shear stress by: 1) Maxwell dissipation with time, and 2) dispersion of the shear stress by transferring it from high to low shear stress. The shear stress change in the damage process is also changed in two ways: 1) transfer of stress to energy by damage or healing, and 2) transfer shear stress to normal stress through the coupling terms $-\gamma\sqrt{I_2}\delta_{ij}$ and $-\gamma(I_1/\sqrt{I_2})\varepsilon_{ij}$ of Eq. (3). The first term is responsible for dilation associated with shear. The inherent difference between the damage and viscous-flow process is that the damage localizes the deformation, whereas viscous-flow tends to spread the deformation. Although we use an exponential low viscosity here, $1/\eta = A\exp(B\tau)$ which localizes the flow, viscous deformation is still dispersive.

The strain partition between the viscous and damage processes depends on the rate of viscous flow controlled by parameters A and B, and the rate of damage controlled by parameters C_d, C_1, and C_2. However, it is questioned if the combination of the two processes might increase the shear strain in some cases where it would be decreased by both processes separately.

Based on seismic velocities at the sinkhole sites we used the following parameters: $\lambda = 1100$ MPa, $\mu_0 = 770$ MPa, $\gamma_r = 920$ MPa, and $\xi_0 = -0.8$ (internal friction angle, $\varphi = 30^0$), $C_d = 50\ s^{-1}$, $C_1 = 1\ s^{-1}$, and $C_2 = 0.005$.

The numerical simulations are done using the Fast Lagrangian Analysis of Continua (FLAC) algorithm (Cundall and Board, 1988; Cundall, 1989; Poliakov et al., 1993; Ilchev and Lyakhovsky, 2001). This fully explicit numerical method relies on a large-strain explicit Lagrangian formulation originally developed by Cundall (1989) for elasto-plastic rheology and implemented in the well-known FLAC 2D software produced by ITASCA. Node coordinates of the numerical mesh are updated every time step as well as shape functions for every triangle element, allowing large strain analyses. Poliakov et al. (1993) developed an adaptive time stepping and applied the FLAC algorithm for visco-elasto-plastic rheology. Their adaptive scheme does not require iteration, which makes the numerical model stable even for highly nonlinear damage rheology (Lyakhovsky et al., 1993).

4. Results

The deformation of the layer that overlies a cavity is modeled with different parameters and different cavity sizes for two-dimensional plane strain cross-sections. The thickness of the layer is set to 20 m for all simulations (the most common depth of the underlying salt layer found by drilling) and the length of the underlying cavity is set to either 10 or 20 m (based on sinkholes average diameter). The visco-elastic parameters of the layer in each simulation are varied from a damage deformation end member ($A = 10^{-16}$ (Pa s)$^{-1}$) to a visco-elastic end member ($A = 10^{-12}$ (Pa s)$^{-1}$). The inter-play between visco-elastic and damage processes is studied at $A = 10^{-14}$–10^{-13} (Pa s)$^{-1}$ when both processes are dominant. Initially, we set the pressure to be lithostatic without any additional tectonic (horizontal) stresses because the weak sediments have relatively short relaxation time on the geological time scale.

4.1. The visco-elastic end member, $A = 10^{-12}$ (Pa s)$^{-1}$

Fig. 3, shows the absolute displacement value for a 10 m-wide cavity. With this low viscosity the layer flows into the cavity. In this case, the resulting surface deformation is a smooth sloping depression above the cavity. This kind of surface deformation has not been observed at the Dead Sea area. In all sinkholes at the Dead Sea, the sinkholes exhibit sharp brittle broken surfaces.

4.2. The damage end member, $A = 10^{-16}$ (Pa s)$^{-1}$

In this case, the flow of the layer is negligible for a time scale of less than a year. All large strain deformations that occur is damage related to shear faulting and tension fractures. Fig. 4 shows the cavity growth into the layer for a 10 m-wide cavity. It takes the damage process 25 days until an $\sim 3.5 \times 10$ m^2 block is ripped from the layer. During this time, damage accumulates along the cavity edges, and propagates upwards until the damage fronts from both sides of the cavity converge and separate the block from the layer. The block is assumed to fall into the underlying cavity. The arching that is formed continues to propagate upwards as pieces from the ceiling fall into the cavity. This propagation stops after 40 days and no more deformation is observed, indicating a stable cavity. The propagation of the ceiling of the cavity is generated in the real world by the irregularity of the layer that is represented by the irregular mesh geometry in the numerical simulation. The shear

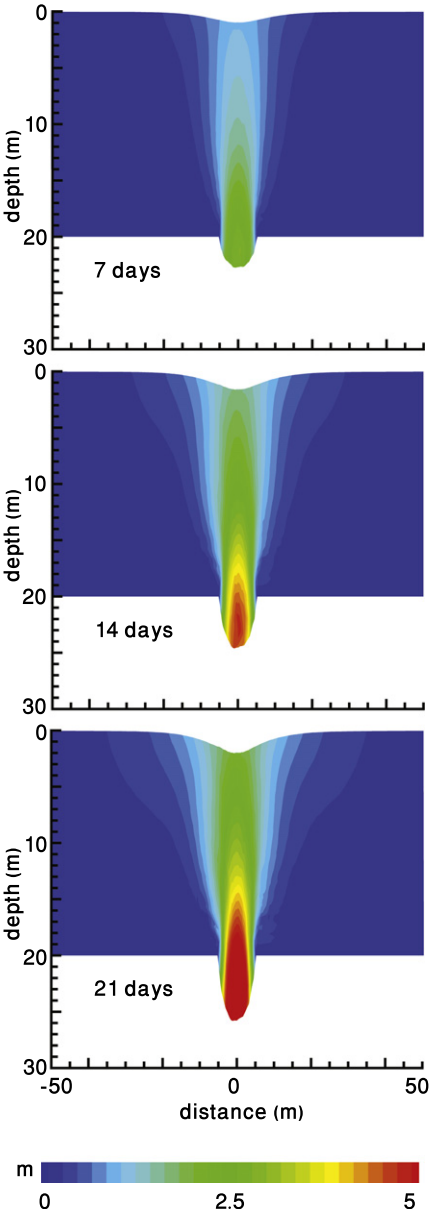

Fig. 3. Absolute displacements for a visco-elastic simulation of deformation caused by a 10 m-wide underlying cavity. No steep walls are created in this process.

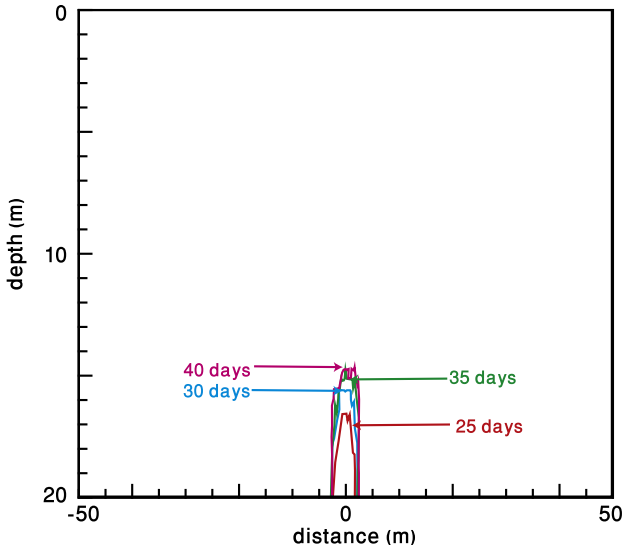

Fig. 4. Cavity configuration evolution for a damage controlled simulation of deformation caused by a 10 m-wide underlying cavity. These results are similar to field observation in the alluvial fans (Fig. 2b).

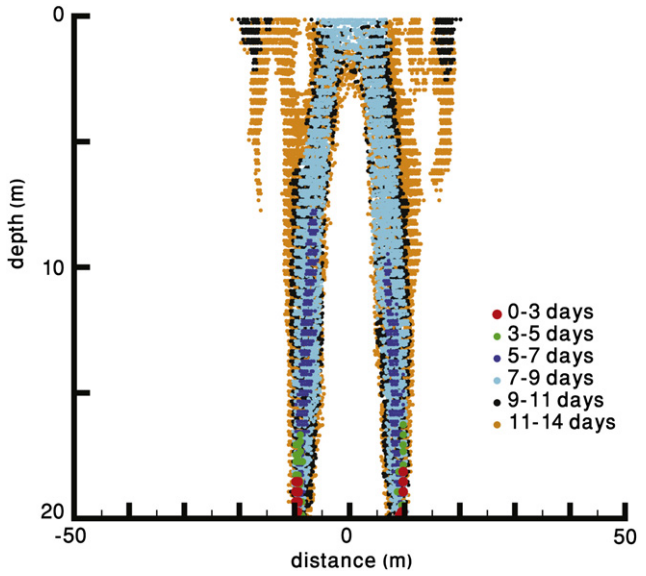

Fig. 5. Micro-seismic events for a damage simulation of deformation triggered by a 20 m-wide underlying cavity. These results are similar to field observation in the alluvial fans (Fig. 2b).

stress is generated by the difference between the stress in the cavity and the layer. The stress in the layer is controlled by the density of the material (ρgz) whereas the stress in the cavity is zero. The arched configuration of the ceiling elastically disperses the shear stress around the cavity, holding failure off. Since the stress in the layer increases with depth, so does the shear stress around a cavity. Therefore, a given arch configuration will be more stable at shallow depths. Fig. 4 shows that the shape of the ceiling remains about the same during propagation, which allows stabilization at shallow depths despite its imperfections. If the material was homogeneous, the cavity would have been stable since it was initially ceiled by arching after 25 days. The surface deformation associated with this process is an elastic deformation of <1 mm. This kind of cavity is predicted to exist for a long time with no surface indication.

A second simulation with the same material properties but with a doubled cavity width (20 m) is shown in Fig. 5. The circles in Fig. 5 represent micro-seismic events where a failure criterion (shear or tension) has been reached and a stress drop was imposed in different periods. The events are nucleated once the damage in an element reaches its critical value and the material looses its resistance for deformation. This element can regain its resistance if it is compacted and healed. Therefore, the same element can experience multiple seismic events. The events are triggered by the shear stress that is introduced by the cavity. They begin at the edges of the cavity and propagate upwards until they each the surface after 9 days. At this point in time, the damage has separated a large block from the layer which is not supported any more. This block collapses into the cavity and creates a sinkhole similar in shape to the one presented in Fig. 2b. The depth of the sinkhole is dictated by the volume available for the block in the cavity. In this simulation we assumed the initial volume of the cavity to be ~ 5 m^2 (depth of 25 cm), and to grow due to material removal by groundwater and by dissolution at a rate of 1.5 m^2/d (velocity of 1 cm/d). The resulting cone-shaped sinkhole is unstable with its negative slopes. In three dimensions this shape is axi-symmetric with some support from the other lateral dimension. The sides of the sinkhole do not support each other anymore. Soon after the block has detached from the layer (9–11 days), events are triggered close to the surface, 20 m from the center of the sinkhole. These events are created by tension failure caused after the main collapse of sinkhole and the lack of support between the two sides of the sinkhole. With time, the events nucleation deepens until finally they reach the sinkhole, creating a stable slope $\theta = 60^0$ that reflects the internal friction angle of the material, $\theta = 45 + 30^\circ/2$. Since in this simulation the initial cavity is small, the detached block falls initially only 25 cm and continues to fall at a velocity of 1 cm/d, the walls of the sinkhole being supported by the subsiding detached block. During its subsidence, the block is episodically attached and detached to the layer by compaction and failure, creating many events while subsiding.

4.3. Intermediate stage, $A = 10^{-14}$ (Pa s)$^{-1}$

Fig. 6 shows the cavity growth with time for an intermediate viscosity and cavity width of 10 m. Similar to the damage end member case, it takes 22 days until a 4×10 m^2 block is ripped from the layer. The arching continues to propagate upwards until day 30. The propagation is much faster than in the damage end-member case because viscous flow is also taking place. When deformation is controlled by viscous flow, imposed cavities are being filled with the surrounding material as shown in the case of the visco-elastic end-member. In this intermediate case, cavities are being formed by the damage process and destroyed by viscous flow. The flow into the cavity at day 30 flattens the arched ceiling and creates unstable elastic conditions. Subsequently, a second collapse rips a block which extends from the cavity and up to the surface. Once the arching is exposed to the surface it becomes unstable and the entire ceiling collapses in the following day, creating vertical walls. A slower process of slope stability decreases the slopes of the sinkholes until they are stable after 50 days at an angle of 60°. This high angle is stable because the sinkhole is still filled with the broken block that supports the sinkhole walls.

Because the visco-elastic process is significant in this case, the surface deformation can be observed beginning already at initial stages (Fig. 7). On day 20 the surface deformation is 7.5 cm. This occurs before the first underground collapse. In fact, the first collapse has no immediate effect on the surface because the visco-elastic stress transfer is relatively slow. However, the visco-

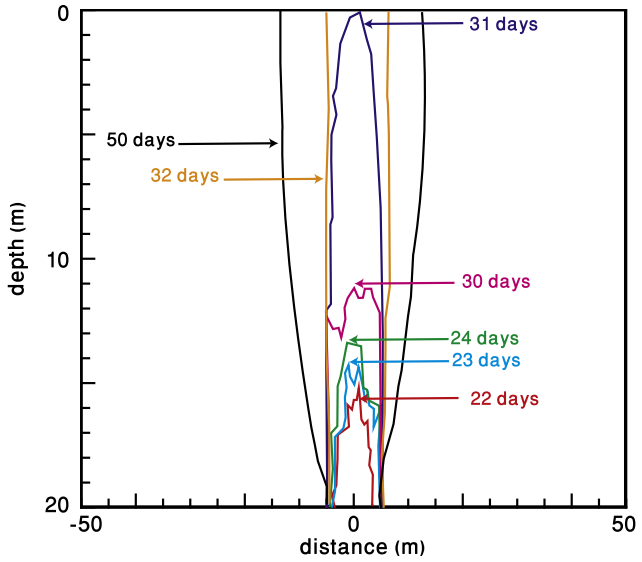

Fig. 6. Cavity configuration evolution for a mixed damage and visco-elastic simulation of deformation caused by a 10 m-wide underlying cavity. These results are similar to field observations in the mud-flat (Fig. 2a).

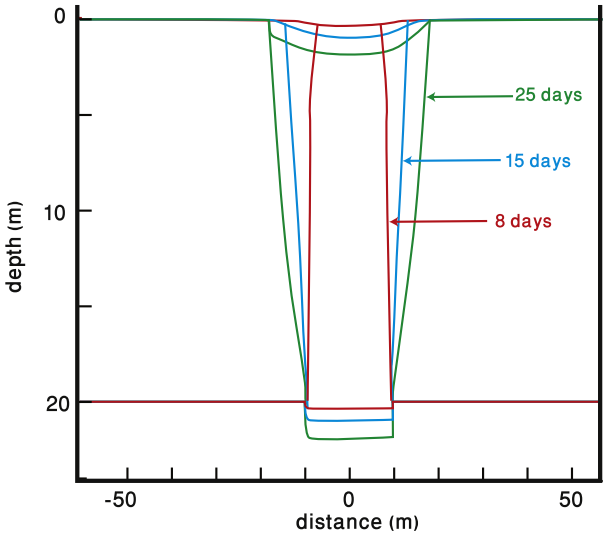

Fig. 8. Cavity configuration evolution for a mixed damage and visco-elastic controlled simulation of deformation caused by a 20 m-wide underlying cavity. These results are similar to field observations in the mud-flat (Fig. 2a).

elasticity indirectly affects surface deformation by destroying the ceiling configuration of the cavity that creates elastic instability, which is transferred much faster to the surface. Because the surface undergoes ductile deformation prior to the collapse this sinkhole is classified as sagging-collapse sinkhole (Gutierrez et al., 2008).

When the cavity width is larger, both processes are faster. Fig. 8 shows that when using the same parameters for a cavity width of 20 m, the collapse of the sinkhole occurs on day 8. This simulation demonstrates the slope evolution of the sinkhole's walls. Once a block is detached from the layer, the amount of its freefall depends on the initial cavity space. Because we chose a relatively small initial cavity space (5 m^2), the freefall of the block is only 25 cm. During the 25 days of this simulation run the cavity grows to a volume of 40 m^2. This growth represents the removal of the cavity fill by groundwater transport and dissolution of the underlying salt layer. The depth of the sinkhole after these 25 days is 2 m. The faults that confine the falling block are episodically healed and damaged during the descent of the block, slowing down its movement. The healing of this process is dictated by compaction of the block and the falls, whereas the damage is dictated by gravity forces that pull the unsupported block.

A different assumption of the size of the initial cavity could result in a sudden complete clearing of the fill. The processes leading to the collapse will be the same for any choice of cavity volume, but the evolution of the sinkhole after breakup will be different. For example, the fractures that define the block are exposed to the surface if the entire block falls down.

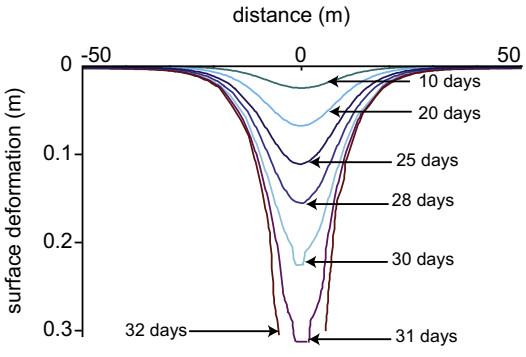

Fig. 7. Surface deformation evolution for a mixed damage and visco-elastic controlled simulation of deformation caused by a 10 m-wide underlying cavity. Because the surface undergoes ductile deformation prior to the collapse this sinkhole is classified as Sagging-Collapse sinkhole. These results are similar to field observations in the mud-flat (Fig. 2a).

5. Discussion

The inter-play between visco-elastic and damage controlled deformation takes place in many Earth Sciences and engineering processes, such as: lithosphere seismic zone, magma flow and cooling, concrete drying, and sinkhole formation. Both visco-elastic and damage processes are triggered by shear stress but are inherently different in nature. The damage process weakens the material and as a result the stress decreases. The energy that was stored as stress is used to destroy the material and is not a part of the stress calculation any more. Shear stress is also transferred to normal stress by the coupling term $-\gamma\sqrt{I_2}\delta_{ij}$ of Eq. (3) that is based on laboratory studies, showing that shear may produce significant normal dilatancy (e.g. Lockner and Byerlee, 1994). Another procedure that is taking place in our numerical modeling of the damage accumulation is nucleation of seismic events and the associated stress drop. Once an element fails, the shear stress that produced the failure is dropped back to below yielding. These three shear stress reduction procedures are all localized at the shear locations and are not transferred to other points.

Viscous-flow dissipates and disperses shear stress. The Maxwell dissipation is a result of the transformation of shear stress to energy which in turn generates material rotation. Similar to damage weakening, this energy is not part of the stress calculation once it is created. However, unlike the damage process, viscous-flow also disperses the shear. The viscosity transfers the shear stress away from high shear stress locations. The distance of viscous-flow, or the radius of rotation, generated by the shear stress depends on the viscosity. For soils, Mitchell and Soga (2005) showed that the viscosity depends exponentially on the shear stress, where the reciprocal of the viscosity is $1/\eta = A\exp(B\tau)$ (Eq. (2)). With high

values of A and B, this relation causes some localization of flow in high sheared locations that decays quickly with distance. However, the nature of the viscous-flow is to disperse the shear. Another difference between viscous flow and damage is that viscous flow acts on any shear stress, whereas damage only acts on shear stress that is above yielding.

The inter-play between the dispersive viscous-flow behavior and localized damage behavior may cause interesting results that do not exist when each process acts separately. For example, viscous-flow and damage processes may divide the stress reduction in a way that reduction of shear stress by viscous-flow suspends damage failure. This is demonstrated by the large number of micro-seismic events in the damage end member case as opposed to the other cases. However, in other cases viscous-flow and damage processes may act together and enhance failure. In the damage end member case, a 3×10 m^2 block is ripped from the layer after 25 days. When viscous-flow is also taking place a larger block, 4×10 m^2 in size, is ripped from the layer after 22 days. In this case, the viscous-flow mechanism increases the damage to the layer. The ability of viscous-flow to enhance or reduce damage depends on the stress distribution. At initial stages, the shear stress that is introduced by the sudden appearance of the cavity is so large that damage is created at a very high rate and all the dispersion of the viscous flow can do is to spread and enlarge damage failure. At later stages, shear stress is reduced and the capability of the viscous flow to disperse the shear before failure is much higher. At a lower shear stress the efficiency of damage accumulation is lower than that of viscous flow because damage is activated only close to yielding.

Another interesting inter-play is the arching stability which is an elastic-damage stable configuration but is unstable visco-elastically. The reason for this is also due to the different triggers of viscous flow and damage respectively. Viscous flow is triggered by any shear stress whereas damage is triggered only when close to failure. The damage process acts to build arches and the viscous flow acts to destroy them. This is illustrated by the intermediate case (Fig. 6). The damage accumulation process builds an arch that confines a block which breaks up from the layer after 22 days. This arch is visco-elastically unstable and triggers material flow that destroys the arch-shaped cavity, which leads to another damage failure of a much larger block.

6. Conclusions

Sinkholes along the Dead Sea coast are shown to mechanically form by both viscous-flow and brittle failure. Sinkholes in the two types of environments: alluvial fans and mud flats are shown to be controlled by brittle failure and viscous flow, respectively. Damage accumulation takes place at all sinkholes including, to some extent, the mud flats sinkholes. This is surprising, given the low viscosity of the Dead Sea mud but may be explained by the existence of some gypsum, halite, or calcite in the mud. On the other hand, the deformation in the alluvial fans may not experience any viscous flow.

The two main inherent differences between viscous flow and damage processes are: 1) viscous flow disperses shear whereas damage localizes shear, and 2) viscous flow is driven by any shear stress, whereas damage deformation is triggered only when close to yielding.

The competition between visco-elastic and damage deformation processes on the stress reduction mechanism may lead to either a magnification or reduction in deformation. It is magnified in high shear stress locations where the dispersion of the viscous flow spreads damage failure, and it is reduced in low shear stress location where viscous flow disperses shear stress before the onset of damage.

Acknowledgments

We would like to thank the editor Cees Passchier as well as the reviewers Mario Parise and an anonymous reviewer, for the thorough evaluations of our manuscript. We appreciate fruitful discussions with Yossi Yechieli, Meir Abelson, Gidi Baer, and Ornit Maimon. This project was funded by GSI project 40393.

References

Abelson, M., Yechieli, Y., Crouvi, O., Baer, G., Wachs, D., Bein, A., Shtivelman, V., 2006. Evolution of the Dead Sea sinkholes. In: Enzel, Y., Agnon, A., Stein, M. (Eds.), New Frontiers in Dead Sea Paleoenvironmental Research. Geological Society of America, vol. 401, pp. 241–253. Special Paper.

Agnon, A., Lyakhovsky, V., 1995. Damage distribution and localization during dyke intrusion. In: Baer, Heimann (Eds.), Physics and Chemistry of Dykes. Balkema, Rotterdam, pp. 65–78.

Augarde, C.E., Lyamin, A.V., Sloan, S.W., 2003. Prediction of undrained sinkhole collapse. J. Geotech. Geoenviron. Engineer. 129, 197–205.

Baryakh, A.A., Fedoseev, A.K., 2011. Sinkhole formation mechanism. J. Mining Sci. 47, 404–412.

Begin, B., Ehrlich, A., Nathan, Y., 1974. Lake Lisan, the pleistocene precursor of the Dead Sea. Geol. Surv. Isr. Bull. 63, 30.

Ben-Avraham, Z., Lyakhovsky, V., Schubert, G., 2010. Drop-down formation of deep basins along the Dead Sea and other strike-slip fault systems. Geophys. J. Int. 181, 185–197.

Byerlee, J.D., 1978. Friction of rocks. Pure Appl. Geophys. 116, 615–626.

Cundall, P.A., 1989. Numerical experiments on localization in frictional materials. Ign. Arch. 59, 148–159.

Cundall, P.A., Board, M., 1988. A microcomputer program for modeling large-strain plasticity problems. In: Swoboda, C. (Ed.), Numerical Methods in Geomechanics. Proc. 6th Int. Conf. Numerical Methods in Geomechanics, Innsbruck. Balkema, Rotterdam, pp. 2101–2108.

Dieterich, J.H., Kilgore, B.D., 1996. Imaging surface contacts; power law contact distributions and contact stresses in quarts, calcite, glass, and acrylic plastic. Tectonophysics 256, 219–239. http://dx.doi.org/10.1016/0040-1951(95)00165-4.

Garfunkel, Z., 1997. The history and formation of the Dead Sea basin. In: Niemi, T.M., Ben-Avraham, Z., Gat, J.R. (Eds.), The Dead Sea: The Lake and its Setting. Oxford University Press, New York, pp. 36–56.

Gutierrez, F., Cooper, A.H., 2002. Evaporite dissolution subsidence in the historic city of Calatayud, Spain, damage appraisal and prevention. Nat. Hazards 25, 259–288.

Gutierrez, F., Guerrero, J., Lucha, P., 2008. A genetic classification of sinkholes illustrated from evaporate paleokarst exposures in Spain. Environ. Geol. 53, 993–1006.

Hamiel, Y., Liu, Y., Lyakhovsky, V., Ben-Zion, Y., Lockner, D., 2004. A visco-elastic damage model with applications to stable and unstable fracturing. Geophys. J. Int. 159, 1155–1165. http://dx.doi.org/10.1111/j.1365-246X.2004.02452.x.

Hamiel, Y., Lyakhovsky, V., Stanchits, S., Dresen, G., Ben-Zion, Y., 2009. Brittle deformation and damage-induced seismic wave anisotropy in rocks. Geophys. J. Int. 178, 901–909. http://dx.doi.org/10.1111/j.1365-246X.2009.04200.x.

Hamiel, Y., Lyakhovsky, V., Ben-Zion, Y., 2011. The elastic strain energy of damaged solids with applications to nonlinear deformation of crystalline rocks. Pure Appl. Geophys. http://dx.doi.org/10.1007/s00024-011-0265-7.

Ilchev, A., Lyakhovsky, V., 2001. Practical aspects of the hybridization of the boundary integral method with damage rheology modeling for the assimilation of seismic data. In: van Aswegen, G., Durrheim, R.J., Ortlepp, W.D. (Eds.), Dynamic Rock Mass Response to Mining, Rockbursts and Seismicity in Mines – RaSiM5. South African Institute of Mining and Metallurgy, Johannesburg, SA, pp. 421–426.

Johnson, P.A., Jia, X., 2005. Non-linear dynamics, granular media and dynamic earthquake triggering. Nature 437, 871–874. http://dx.doi.org/10.1038/nature04015.

Lockner, D.A., Byerlee, J.D., 1994. Dilatancy in hydraulically isolated faults and the suppression of instability. Geophys. Res. Lett. 21, 2353–2356.

Lyakhovsky, V., Hamiel, Y., Ben-Zion, Y., 2011. A non-local visco-elastic damage model and dynamic fracturing. J. Mech. Phys. Solids 59, 1752–1776. http://dx.doi.org/10.1016/j.jmps.2011.05.016.

Lyakhovsky, V., Ben-Zion, Y., Agnon, A., 1997. Distributed damage, faulting, and friction. J. Geophys. Res. 102, 27,635–27,649.

Lyakhovsky, V., Podladchikov, Y., Poliakov, A., 1993. Rheological model of a fractured solid. Tectonophysics 226, 187–198.

Manspeizer, W., 1985. The Dead Sea rift: impact of climate and tectonism on pleistocene and holocene sedimentation. In: Biddle, K.T., Christie-Blick, N. (Eds.), Strike Slip Deformation, Basin Formation, and Sedimentation. Society of Economic Paleontologists and Mineralogists Special Publication, vol. 37, pp. 143–158.

Martinez, J.D., Johnson, K.S., Neal, J.T., 1998. Sinkholes in evaporite rocks. Amer. Sci. 85, 38–51.

Mitchell, J.K., Soga, K., 2005. Fundamentals of Soil Behavior, third ed. John Wiley & Sons, Inc, 558 pp.

Poliakov, A., Cundall, P., Podladchikov, Y., Lyakhovsky, V., 1993. An explicit inertial method for the simulation of viscoelastic flow: an evaluation of elastic effects

on diapiric flow in two- and three-layers model. In: Runcorn, K.E., Stone, D. (Eds.), Dynamic Modeling and Flow in the Earth and Planets. Proceedings of the NATO Advanced Study Institute. Kluwer, Dordrecht, pp. 175–195.
Parise, M., 2008. Rock failures in karst. In: Cheng, Z., Zhang, J., Li, Z., Wu, F., Ho, K. (Eds.), Landslides and Engineered Slopes. Proc. 10th International Symposium on Landslides, Xi'an (China), June 30 – July 4, 2008, vol. 1, pp. 275–280.
Parise, M., Lollino, P., 2011. A preliminary analysis of failure mechanisms in karst and man-made underground caves in Southern Italy. Geomorphology 134, 132–143.
Sagy, A., Reches, Z., Agnon, A., 2003. Multiscale 3D architecture and mechanics of the margins of the Dead Sea pull-apart. Tectonics 22, 1004. http://dx.doi.org/10.1029/2001TC001323.
Scholz, C.H., 2002. The Mechanics of Earthquakes and Faulting, second ed., 471 pp.
Shalev, E., Lyakhovsky, V., Yechieli, Y., 2006. Salt dissolution and sinkhole formation along the Dead Sea shore. J. Geophys. Res. 111. http://dx.doi.org/10.1029/2005JB004038
Sneh, A., 1979. Late pleistocene fan deltas along the Dead Sea rift. J. Sedimentary Petrol. 49, 541–552.
Tharp, T.M., 1999. Mechanics of upward propagation of cover-collapse sinkholes. Eng. Geol. 52, 23–33.
Waltham, T., Bell, F.G., Culshaw, M.G., 2005. Sinkholes and Subsidence: Karst and Cavernous Rocks in Engineering and Construction. Springer Praxis Publishing, Chichester, UK, 379 pp.
Yechieli, Y., Magaritz, M., Levy, Y., Weber, U., Kafri, U., Woelfl, I.W., Bonani, G., 1993. Late quaternary geological history of the Dead Sea area, Israel. Quaternary Res. 39, 59–67. http://dx.doi.org/10.1006/qres.1993.1007.
Yechieli, Y., Abelson, M., Bein, A., Crouvi, O., Shtivelman, V., 2006. Sinkhole "swarms" along the Dead Sea coast: reflection of disturbance of lake and adjacent groundwater systems. Geol. Soc. America Bull. 118, 1075–1087.
Zak, I., 1967. The geology of Mount Sedom, Ph.D. thesis. The Hebrew University, 208 p. (in Hebrew, with English summary).